PHYSICAL REVIEW C **80**, 051304(R) (2009)

# Characterization of superdeformed bands in $^{62}$Zn

J. Gellanki,[1,*] I. Ragnarsson,[2] D. Rudolph,[1] C. E. Svensson,[3] L.-L. Andersson,[1,†] C. Andreoiu,[1,3,‡] C. Baktash,[4] M. P. Carpenter,[5] R. J. Charity,[6] C. J. Chiara,[6,§] J. Eberth,[7] J. Ekman,[1,‖] C. Fahlander,[1] D. S. Haslip,[3] E. K. Johansson,[1] D. R. LaFosse,[6,¶] S. D. Paul,[4] O. L. Pechenaya,[6,**] W. Reviol,[6] R. du Rietz,[1,††] D. G. Sarantites,[6] D. Seweryniak,[5] L. G. Sobotka,[6] H. G. Thomas,[7] D. A. Torres,[1,8,‡‡] J. C. Waddington,[3] J. N. Wilson,[6,§§] C. H. Yu,[4] and S. Zhu[5]

[1]*Department of Physics, Lund University, S-22100 Lund, Sweden*
[2]*Division of Mathematical Physics, LTH, Lund University, S-22100 Lund, Sweden*
[3]*Department of Physics, University of Guelph, Guelph, Ontario N1G 2W1, Canada*
[4]*Physics Division, Oak Ridge National Laboratory, Oak Ridge, Tennessee 37831, USA*
[5]*Physics Division, Argonne National Laboratory, Argonne, Illinois 60439, USA*
[6]*Chemistry Department, Washington University, St. Louis, Missouri 63130, USA*
[7]*Institut für Kernphysik, Universität zu Köln, D-50937 Köln, Germany*
[8]*Departamento de Física, Universidad Nacional de Colombia, Bogotá, Colombia*

(Received 18 September 2009; published 24 November 2009)

Combined data from four fusion-evaporation reaction experiments were utilized to investigate deformed and superdeformed structures in $^{62}_{30}Zn_{32}$. Combination of the Gammasphere $\gamma$-ray spectrometer and ancillary particle detection systems allowed for the connection of rotational bands to well-known, low-lying excited states in $^{62}$Zn, as well as spectroscopy of discrete high-spin states reaching excitation energies of $E_x = 42.5$ MeV. Four well- or superdeformed bands in $^{62}$Zn are characterized and described by means of cranked Nilsson-Strutinsky calculations.

DOI: 10.1103/PhysRevC.80.051304 PACS number(s): 21.60.Cs, 23.20.En, 23.20.Lv, 27.50.+e

The existence of nuclear rotational excitations relates directly to the possible nonisotropic mass distribution of the nucleus. Indeed, some nuclei are found to have a stable axial deformation with a major-to-minor axis ratio approaching 2 : 1. Nuclei at this extraordinary deformation are referred to as "superdeformed" (SD), and more than 250 SD bands have been observed in the mass regions $A \sim 190$, 150, 130, 80, 60, and 40 [1]. Building on two-particle, two-hole (2p-2h) excitations for both protons and neutrons across the magic gap at particle numbers $Z = N = 28$, large SD shell gaps at single-particle energy levels for the particle numbers $N, Z \sim$ 30–32 were predicted in the $A \sim 60$ mass region long ago [2,3]. In the intermediate spin and energy range, these SD bands often compete with well-deformed (WD) terminating bands, which have a smaller number of cross-shell excitations.

Following the first observation of an SD band in $^{62}$Zn [4], SD bands and, likewise, WD bands have been observed in a number of nuclei in the $A \sim 60$ region, namely, $^{57}$Co [5], $^{56,58-60}$Ni [6–11], $^{58,59,61}$Cu [12–16], and $^{60-62}$Zn [17–20]. Despite significant experimental information on $^{62}$Zn, the properties of the SD band in $^{62}$Zn remain unclear [4,21]. The decay-out transitions of the SD band could not be established [4], which was taken to signify a different decay-out process compared to $^{60,61}$Zn [17,18]. The additional neutrons outside the $N = 30$ shell gap may affect both pair correlations and the barrier between the SD well and the first, near-spherical potential well. In this study, we were able to classify the known and three new rotational bands in $^{62}$Zn.

The results originate from the combined statistics of four experiments carried out at Argonne and Lawrence Berkeley National Laboratory. For a thorough description of the experimental details, see, for example, Refs. [9,11,14,19]. In brief, one experiment used the fusion-evaporation reaction $^{40}$Ca($^{28}$Si,1$\alpha$2$p$)$^{62}$Zn at a beam energy of 122 MeV. The target with 99.975% isotopic enrichment was 0.5 mg/cm$^2$ thick. $^{62}$Zn nuclei were populated with ≈30% of the total fusion-evaporation cross section. The experimental setup consisted of the Gammasphere array [22], at that time comprising 103 Ge detectors, for $\gamma$-ray detection. The array was operated in conjunction with the $4\pi$ charged-particle detector array Microball [23]. The Heavimet collimators were removed from the Ge detectors to provide $\gamma$-ray multiplicity and sum-energy measurements [24] and additional channel selectivity by total energy conservation requirements [25]. `Data set 1` represents the basis of our study, namely, to identify the SD bands and the decay-out transitions from the SD bands into states in the first minimum of the potential. In

*gellanki.jnaneswari@nuclear.lu.se
†Present address: Department of Physics, University of Liverpool, Liverpool L69 7ZE, United Kingdom.
‡Present address: Chemistry Department, Simon Fraser University, Burnaby, British Columbia V5A 1S6, Canada.
§Present address: Nuclear Engineering Division, Argonne National Laboratory, Argonne, Ilinois 60439, USA.
‖Present address: Malmö högskola, S-20506 Malmö, Sweden.
¶Present address: Teradyne Inc., North Reading, Massachusetts 01864, USA.
**Present address: Department of Radiation Oncology, Washington University School of Medicine, St. Louis, Missouri 63130, USA.
††Present address: Department of Nuclear Physics, The Australian National University, Canberra, ACT 0200, Australia.
‡‡Present address: University of the West of Scotland, High Street, Paisley PA1 2BE, Scotland, United Kingdom.
§§Present address: IPN Orsay, F-91406 Orsay, France.

 

addition, three more experiments using the fusion-evaporation reaction $^{28}$Si($^{36}$Ar,2$p$)$^{62}$Zn at beam energies of about 140 MeV were performed [9,11,19]. Whereas the relative yield for $^{62}$Zn is very small, this combined `data set 2` adds to the addition of the highest-spin states of the bands.

The analysis was restricted to events in which all of the evaporated charged particles, that is, two protons in the case of `data set 2` and an additional $\alpha$ particle for `data set 1`, were detected. A kinematic Doppler-shift correction of the $\gamma$-ray energies is possible, based on the measured charged-particle energies and directions, which define the momenta of the recoiling residual nuclei for each event. In addition, the $\gamma$ rays originating from the SD bands are likely to be emitted while the residual $^{62}$Zn nuclei are still slowing down inside the thin target foil. Assuming average deformation of the rotational bands in $^{62}$Zn and simulating the slowing-down process in the thin target layer, so-called additional fractional Doppler shifts can be derived as a function of $\gamma$-ray energy [26]. Taking this into account, a more accurate Doppler-shift correction of the $\gamma$ rays originating from deformed structures is obtained.

Our study of $^{62}$Zn relies on a $\gamma\gamma\gamma$ cube of `data set 1` analyzed with the RADWARE package [27]. To confirm low-intensity or ambiguous transitions, certain parts of the decay scheme are focused on during the analysis by specific $\gamma\gamma$ matrices, which are preselected by $\gamma$ rays originating from a certain rotational band or decay sequence within the complex $^{62}$Zn excitation scheme. For `data set 2`, a $\gamma\gamma$ matrix was created, which focuses on the high-lying entry states in $^{62}$Zn by requiring at least 14 detected $\gamma$ rays with at least 16.5-MeV total energy and less than 19-MeV particle energy [8]. For $\gamma$-ray spectrum analyses, the code TV developed at the University of Cologne [28] was used. The assignment of $E1$, $M1$, $E2$, or mixed $E2/M1$ multipolarities to $\gamma$-ray transitions is based on directional correlations from oriented states defined as the ratio of yields, $Y$:

$$R_{\mathrm{DCO}} = \frac{Y(\gamma_1 \text{ at } 30^\circ;\ \text{gated with } \gamma_2 \text{ at } 83^\circ)}{Y(\gamma_1 \text{ at } 83^\circ;\ \text{gated with } \gamma_2 \text{ at } 30^\circ)}.$$

Using known stretched $E2$ transitions as $\gamma_2$, $R_{\mathrm{DCO}} \sim 1.0\,(0.6)$ is expected for observed quadrupole (dipole) transitions $\gamma_1$. For more details, we refer to, for example, Refs. [14] and [16].

The primary result of the coincidence analysis is the high-spin excitation scheme of $^{62}$Zn shown in Fig. 1. Four bands, labeled SD1, SD2, SD3, and WD1, are observed, whereas only the most relevant transitions in the complex low-lying decay scheme of $^{62}$Zn are included [4,20,29]. All four bands are connected to the low-spin states by several linking transitions. This allows spin and parity assignments to the lowest states in the bands, because the transitions at the bottom of the bands are either sufficiently intense or sufficiently clean to distinguish between stretched quadrupole and dipole characters of some of the more intense linking transitions. Assuming an $E2$ character of the in-band transitions, the tentative spin and parity assignments to the states near the top of the bands are based on their regular rotational behavior.

The known band SD1, which was observed up to the 3234-keV transition [4], was extended by transitions at 3579, 3958, and 4234 keV. These topmost transitions are observed only in `data set 2`: the spectrum in Fig. 2(b) was obtained by summing $\gamma$-ray spectra in coincidence with several SD1 band members in the corresponding two-proton selected $\gamma\gamma$ matrix. Whereas both the 3958- and the 4234-keV transitions are found to be in coincidence with the line at 3579 keV, a mutual coincidence between them cannot be firmly established. Thus the 4234-keV line is not included in Fig. 1, as it feeds either the 36496- or the 40454-keV level of SD1.

Figure 2(a) shows results for SD1 from the high-statistics `data set 1`. SD1 is connected to the low-spin part of the level scheme via a total of six $\gamma$-ray transitions. Interestingly, all of them feed "band 2" of Ref. [20], and some of them are labeled in Fig. 2(a), at 2963, 3027, and 3983 keV. These are clearly visible, even though their relative yield is only ~0.1% of the 954-keV ground-state transition. Low-lying SD1 band members are about a factor of 10 more "intense," consistent

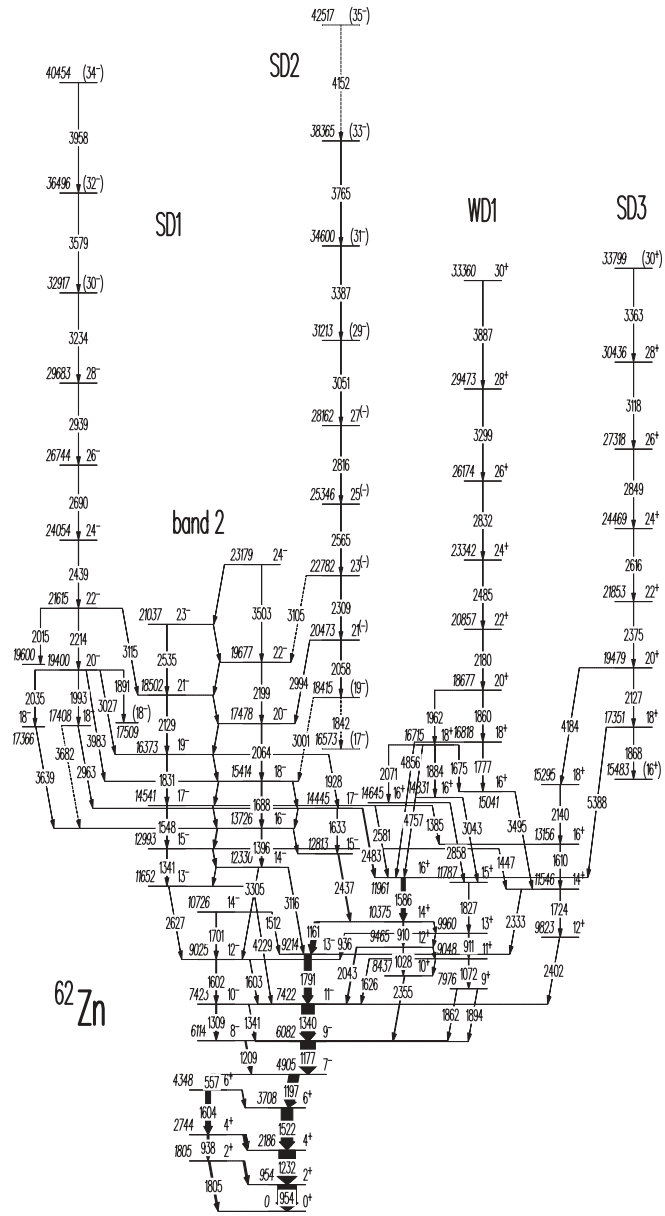


FIG. 1. Partial decay scheme of $^{62}$Zn. Energy values are given as kilo-electron volts, and the widths of the arrows correspond to the relative intensities of the $\gamma$ rays.

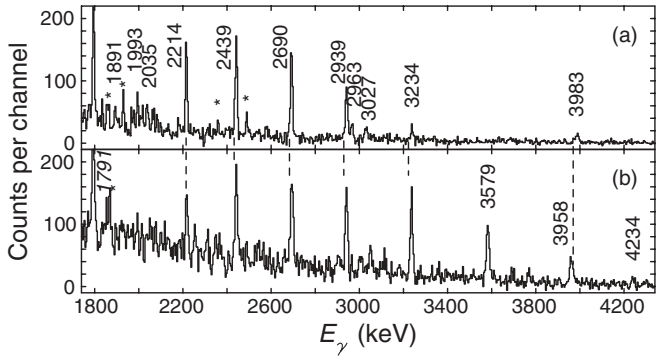


FIG. 2. (a) $\gamma$-ray spectrum in coincidence with any combination of two of the 1993-, 2214-, 2439-, 2690-, 2939-, and 3234-keV transitions of SD1 taken from `data set 1`. (b) $\gamma$-ray spectrum generated from `data set 2` by coincidence requirements on the 2214-, 2439-, 2690-, 2939-, 3234-, and 3579-keV transitions in SD1. $\gamma$-ray labels are kilo-electron volts, the binning is 4 keV per channel, and an asterisk or italic labeling indicates lines from the lower part of the $^{62}$Zn decay scheme in Fig. 1.

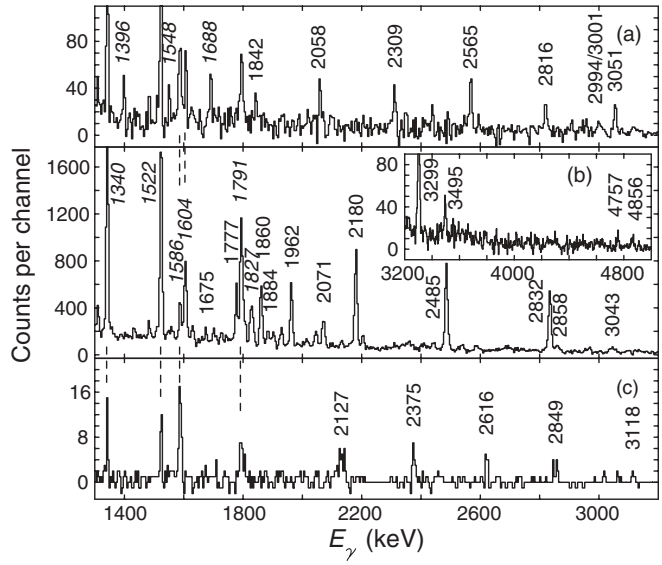


FIG. 3. A sample of $\gamma$-ray spectra taken from `data set 1`. (a) Spectrum in coincidence with any combination of the 2309-, 2565-, and 2816-keV and the 1842-, 2058-, 2309-, 2565-, 2816-, and 3051-keV transitions of SD2. (b) Spectrum in coincidence with any combination of the 2180-, 2485-, 2832-, and 3299-keV and the 1860-, 1962-, 2180-, 2485-, 2832-, and 3299-keV transitions of WD1. (c) Spectrum in coincidence with the 5388-keV decay-out transition and any of the 2375-, 2616-, 2849-, and 3118-keV transitions of SD3. See text and caption to Fig. 2 for more details.

with Ref. [4]. Despite this very low yield, a careful analysis provides $R_{\rm DCO} = 0.59(24)$ and $R_{\rm DCO} = 1.12(36)$ for the 2963- and 3983-keV lines, respectively. In conjunction with the $E2$ character of the in-band transitions, these numbers provide the $I^\pi = 20^-$ assignment of the 19400-keV level. Thus, the maximum observed spin of SD1 is $I^\pi = (34^-)$ at an excitation energy of $E_x = 40.7$ MeV. Note that the high statistics allow for observation of the beginning of several decay-out branches near the bottom of SD1, for example, the yield of the 1891-, 1993-, and 2035-keV transitions accounting essentially for that of the 2214-keV line.

Excitation energies and rotational frequencies of SD1 and the bands in $^{58}$Ni [8] are surpassed by SD2, which is shown in Fig. 3(a). Like SD1, the three topmost transitions, at 3387, 3765, and 4152 keV, are seen only in `data set 2`. The transitions linking SD2 into "band 2" [4] are established at 2994 keV and, tentatively, 3001 and 3105 keV. In addition, the DCO ratio of the doublet at 2994/3001 keV amounts to $R_{\rm DCO} = 0.61(20)$, that is, dipole character. The parity assignment for SD2 remains tentative, as it is impossible to distinguish electric or magnetic dipole character with the present data.

Figure 3(b) illustrates WD1 as obtained from `data set 1`. The inset shows the high-energy part of the spectrum. Once more the topmost transition at 3887 keV is only observed in `data set 2`. With an intensity of about 2% relative to the 954-keV ground-state transition, WD1 is presently the most intense high-spin band in $^{62}$Zn. The band is connected to low-spin states via several linking paths including transitions at 1827, 1884, 2858, 3043, 3495, 4757, and 4856 keV. Among these, the 3043- to 1827-keV cascade (dipole-quadrupole) and the 3495-keV direct link (quadrupole) are intense enough to deduce DCO ratios [29]. Thus, positive parity can be assigned to WD1.

A spectrum in coincidence with the 5388-keV decay-out transition of SD3 and one of the band members of SD3 is shown in Fig. 3(c). It provides the extremely high quality of `data set 1`: With relative yields as low as 0.02% (5388-keV line) and less than 0.8% (band members), the triple coincidences both with members of SD3 (2127, 2375, 2616, 2849, and 3118 keV) and with the relevant transitions in the low-spin regime (here 1340, 1522, 1586, and 1791 keV) are clearly visible. The DCO ratio for the 5388-keV linking transition is found to be consistent with $E2$ character [$R_{\rm DCO} = 1.15(34)$], that is, the maximum spin of this band is $I^\pi = (30^+)$ at $E_x = 33.8$ MeV.

Observed bands were analyzed using the configuration-dependent cranked Nilsson-Strutinsky model [30–32]. In this model, one considers the rotation from the intrinsic frame of reference, in which nucleons experience an additional potential caused by the Coriolis and centrifugal forces. The total energy of fixed configurations is minimized in the deformation parameters $\varepsilon_2$, $\gamma$, and $\varepsilon_4$ at each spin. Standard parameters [30] were used in the Nilsson Hamiltonian. At high spin, pairing is of little importance and thus neglected.

Configurations assigned to the observed SD bands in $^{62}$Zn are illustrated schematically in Fig. 4. The most important orbitals include the $\mathcal{N} = 3$ high-$j$ shell $1f_{7/2}$ and upper $fp$-shell orbitals $1f_{5/2}$, $2p_{3/2}$, and $2p_{1/2}$ and, finally, the $\mathcal{N} = 4$ orbit $1g_{9/2}$. In the deformed rotating potential these $j$ shells mix, that is, the wave functions of the single-particle orbitals will have amplitudes in several $j$ shells. However, it turns out that for deformations up to $\varepsilon_2 = 0.3$–$0.4$, the orbitals can be classified as having their main amplitudes either in the high-$j$ intruder shell or in the other shells with lower $j$ values [31,33]. Thus, each configuration can be labeled $[p_1 p_2, n_1 n_2]$. Here, for protons and neutrons, respectively, $p_1$ and $n_1$ denote the number of holes in the high-$j$ $1f_{7/2}$ orbitals, and $p_2$ and $n_2$ denote the number of particles in the high-$j$ $1g_{9/2}$ subshell.

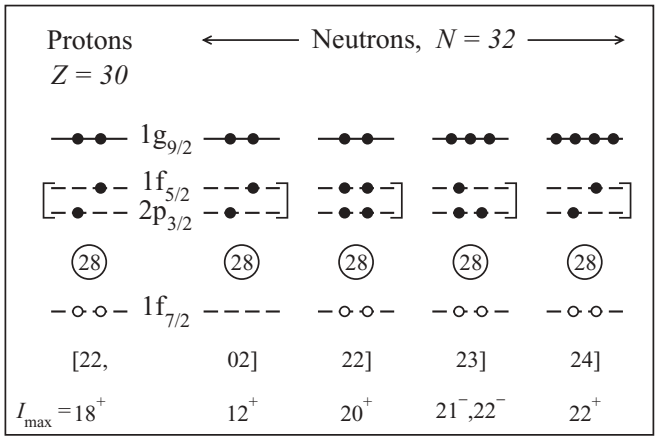


FIG. 4. Schematic illustration of configurations considered for interpretation of the observed SD bands in $^{62}$Zn. Filled circles indicate particles and open circles indicate holes relative to the spherical $Z = N = 28$ gap. The $2p_{3/2}$ and $1f_{5/2}$ subshells are coupled to indicate that they mix strongly and are therefore treated as one entity in the configuration assignment. The $I_{\max}$ value given below each configuration is the maximum spin value that can be formed for the pure configuration according to the Pauli principle.

The valence configuration of $^{62}$Zn corresponds to $\pi(2p_{3/2}1f_{5/2})^2\nu(2p_{3/2}1f_{5/2})^4$, namely, [00,00] in short-hand notation. Higher excitations for both 30 protons and 32 neutrons are obtained by lifting particles across the $Z = N = 28$ spherical shell gaps from the $1f_{7/2}$ subshell and/or exciting them to the $1g_{9/2}$ high-$j$ shell. The combination of such proton and neutron excitations gives rise to the SD band configurations shown in Fig. 5. For example, in the case of protons, lifting the two particles from $1f_{7/2}$ into $1g_{9/2}$ yields the configuration $\pi(1f_{7/2})^{-2}(1f_{5/2}2p_{3/2})^2(1g_{9/2})^2$ with maximum spin, $I_{\max} = 18^+$, labeled "[22]." This proton configuration is greatly favored in a large region of the deformation space and relates to the doubly magic SD band in the $Z = N = 30$ nucleus $^{60}_{30}$Zn [17]. Above the corresponding neutron $N = 30$ SD gap, there are signature $\alpha = \pm 1/2$ pairs of low-$j$ and high-$j$ $\mathcal{N} = 3$ orbitals as well as high-$j$ $\mathcal{N} = 4$ orbitals at similar energies. It becomes possible to form a rather large number of roughly equally favored configurations. The ones most likely to be assigned to the observed SD bands are shown in Fig. 4. Also note that because these low-$j$ and high-$j$ $\mathcal{N} = 3$ orbitals come at a similar energy, they mix rather strongly and special care must be taken to distinguish the different configurations [29].

In Fig. 5, the experimental bands are compared with the cranked Nilsson-Strutinsky predictions The energy difference between observed and calculated bands shown in the lower panels are expected to come within about ±1 MeV. If the observed transition energies are predicted correctly for the transitions within a band, the corresponding curve in the bottom panel will have a constant energy difference.

Bands SD1 and SD2 are signature partners with negative parity, which implies an odd number of $1g_{9/2}$ particles. This leaves [22,23] and [22,13] as possible assignments. The [22,23] configuration is clearly the most likely interpretation: it is calculated ∼1 MeV lower in energy and it appears

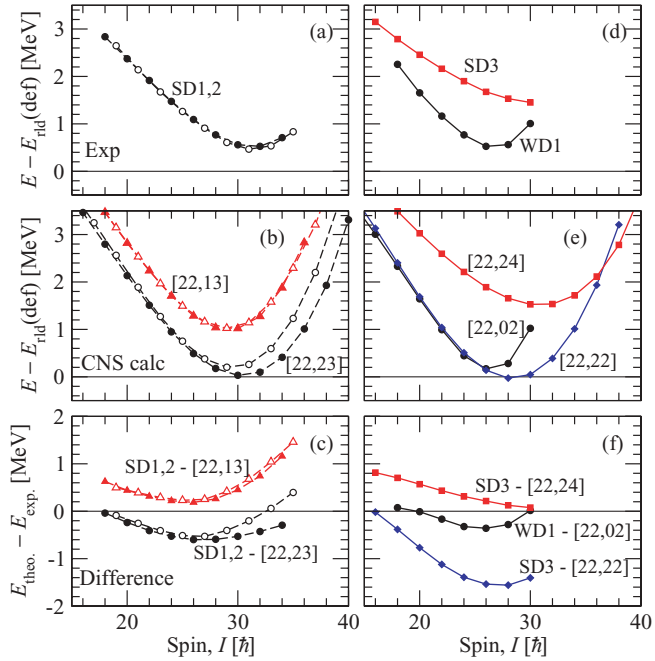


FIG. 5. (Color online) Comparison between experimentally observed structures and cranked Nilsson-Strutinsky predictions for rotational bands in $^{62}$Zn, with the absolute energy scale fixed according to Ref. [32]. Top panels illustrate experimental energies relative to the rotating liquid drop (rld) energy, where the bands are labeled according to Fig. 1. Middle panels show the selected calculated bands. Bottom panels plot the energy difference between the predictions and the observations. Signature $\alpha = 0$ is represented by filled symbols; $\alpha = 1$, by open symbols. Solid (dashed) lines represent positive (negative) parity.

impossible to get [22,13] below [22,23] with reasonable parameter changes. As shown in Fig. 5, the absolute energy of the [22,23] configuration is in good agreement with experiment, whereas the [22,13] configuration deviates too much at high spin. On the other hand, the two signatures are almost degenerate up to the highest spin values observed in experiment, which is in general agreement with the [22,13] but not with the [22,23] configuration. Therefore, we cannot totally exclude [22,13] as a possible assignment for SD1 and SD2. Both SD1 and SD2 decay-out primarily via "band 2," which has a [11,02] assignment [20]. Because band 2 falls in between the SD well and the near-spherical well, in terms of energy, spin, and deformation, a stepwise decay-out mechanism can be inferred for $^{62}$Zn, similar to other $N \neq Z$ nuclei in the region [11,15,16,19].

WD1 is in good agreement with the [22,02] configuration. Though observed to its maximum spin value, it is still calculated to be slightly collective at $I = I_{\max}$, similar to bands discussed in Ref. [34]. The steep up slope when approaching $I = 30$ gives strong support for this assignment.

For SD3, configurations [22,22] or [22,24] are the most likely assignments. The general behavior of the curves in the lower panel in Fig. 5 is similar to that of the [22,22] assignment and the other observed bands. On the contrary, the absolute value of the difference is much larger than for the [22,24] assignment. However, with the [22,24] assignment, it

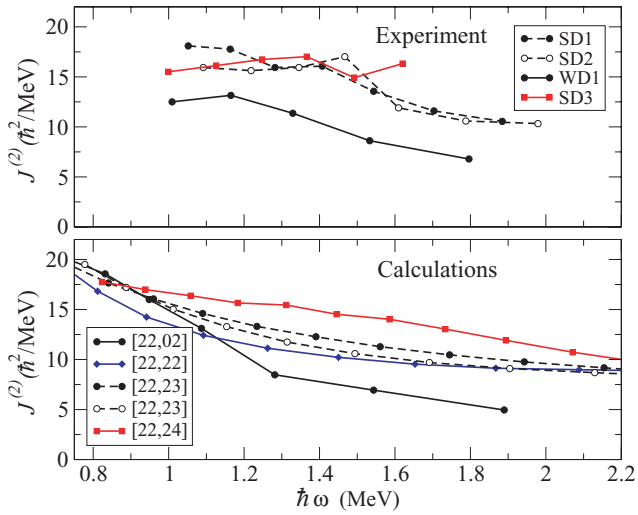


FIG. 6. (Color online) $J^{(2)}$ moments of inertia vs. rotational frequency for both observed and calculated rotational bands in $^{62}$Zn.

is remarkable that the [22,22] band has not yet been observed, as it is calculated to be lower in energy.

The $J^{(2)}$ moments of inertia of the observed bands are shown in Fig. 6. Partly based on $J^{(2)}$ values, configuration [22,24] was assigned to SD1 in Ref. [21]. However, with the band itself extended to a higher spin, and in view of the observed signature partner, a [22,23] configuration assignment is now more reasonable also from the point of view of $J^{(2)}$ moments of inertia. On the contrary, based solely on the $J^{(2)}$ value, [22,13] is another possible assignment because it has a very similar curvature in Fig. 5(b) and, thus, a very similar $J^{(2)}$ (not shown in Fig. 6). The low value of $J^{(2)}$ for WD1 and configuration [22,02] reflects the large curvature in the upper panels in Fig. 5. Finally, SD3 is not observed at frequencies high enough to give any clear configuration preference related to $J^{(2)}$ values.

In summary, combining data from several fusion-evaporation reaction experiments using the Gammasphere finally allowed solving of the configuration assignment puzzle of the very first $A \sim 60$ SD band in $^{62}$Zn [4,21]. Three more SD bands were experimentally observed in $^{62}$Zn, two of which were also readily characterized by means of cranked Nilsson-Strutinsky calculations.

We would like to thank the accelerator crews and the Gammasphere support staff at Argonne and Berkeley for their superb efforts.

[1] B. Singh, R. Zywina, and R. B. Firestone, Nucl. Data Sheets **97**, 241 (2002).
[2] I. Ragnarsson, S. G. Nilsson, and R. K. Sheline, Phys. Rep. **45**, 1 (1978).
[3] J. Dudek, W. Nazarewicz, Z. Szymanski, and G. A. Leander, Phys. Rev. Lett. **59**, 1405 (1987).
[4] C. E. Svensson *et al.*, Phys. Rev. Lett. **79**, 1233 (1997).
[5] W. Reviol *et al.*, Phys. Rev. C **65**, 034309 (2002).
[6] D. Rudolph *et al.*, Phys. Rev. Lett. **82**, 3763 (1999).
[7] E. K. Johansson *et al.*, Phys. Rev. C **77**, 064316 (2008).
[8] D. Rudolph *et al.*, Phys. Rev. Lett. **96**, 092501 (2006).
[9] E. K. Johansson *et al.*, Phys. Rev. C **80**, 014321 (2009).
[10] C.-H. Yu *et al.*, Phys. Rev. C **65**, 061302(R) (2002).
[11] D. A. Torres *et al.*, Phys. Rev. C **78**, 054318 (2008).
[12] D. Rudolph *et al.*, Phys. Rev. Lett. **80**, 3018 (1998).
[13] C. Andreoiu *et al.*, Phys. Rev. C **62**, 051301(R) (2000).
[14] C. Andreoiu *et al.*, Eur. Phys. J. A **14**, 317 (2002).
[15] C. Andreoiu *et al.*, Phys. Rev. Lett. **91**, 232502 (2003).
[16] L.-L. Andersson *et al.*, Eur. Phys. J. A **36**, 251 (2008).
[17] C. E. Svensson *et al.*, Phys. Rev. Lett. **82**, 3400 (1999).
[18] C.-H. Yu *et al.*, Phys. Rev. C **60**, 031305(R) (1999).
[19] L.-L. Andersson *et al.*, Phys. Rev. C **79**, 024312 (2009).
[20] C. E. Svensson, C. Baktash, G. C. Ball, J. A. Cameron, M. Devlin, J. Eberth, S. Flibotte, A. Galindo Uribarri, and D. S. Haslip, Phys. Rev. Lett. **80**, 2558 (1998).
[21] A. V. Afanasjev, I. Ragnarsson, and P. Ring, Phys. Rev. C **59**, 3166 (1999).
[22] I.-Y. Lee, Nucl. Phys. **A520**, 641c (1990).
[23] D. G. Sarantites *et al.*, Nucl. Instrum. Methods Phys. Res. A **381**, 418 (1996).
[24] M. Devlin *et al.*, Nucl. Instrum. Methods Phys. Res. A **383**, 506 (1996).
[25] C. E. Svensson *et al.*, Nucl. Instrum. Methods Phys. Res. A **396**, 228 (1997).
[26] B. Cederwall *et al.*, Nucl. Instrum. Methods Phys. Res. A **354**, 591 (1995).
[27] D. C. Radford, Nucl. Instrum. Methods Phys. Res. A **361**, 297 (1995).
[28] J. Theuerkauf *et al.*, program TV, University of Cologne (unpublished).
[29] J. Gellanki *et al.* (to be published).
[30] T. Bengtsson and I. Ragnarsson, Nucl. Phys. **A436**, 14 (1985).
[31] A. V. Afanasjev, D. B. Fossan, G. J. Lane, and I. Ragnarsson, Phys. Rep. **322**, 1 (1999).
[32] B. G. Carlsson and I. Ragnarsson, Phys. Rev. C **74**, 011302(R) (2006).
[33] I. Ragnarsson, V. P. Janzen, D. B. Fossan, N. C. Schmeing, and R. Wadsworth, Phys. Rev. Lett. **74**, 3935 (1995).
[34] J. J. Valiente-Dobon *et al.*, Phys. Rev. Lett. **95**, 232501 (2005).